DOI: 10.2478/auoc-2025-0019

Ovidius University Annals of Chemistry Volume 36, Issue 2, pp. 162 - 169, 2025

Specific capacitance and electrochemical properties of charge transfer complex of 4,4'-bipyridine with a benzoquinone derivative

Ibrahim EL-HALLAG[*],[1] Ahmad AL-OWAIS,[2] and El-Sayed EL-MOSSALAMY[3]

[1]*Chemistry Department, Faculty of Science, Tanta University, Al-Geish St., Gharbia, Tanta, Egypt*
[2]*Chemistry Department, Faculty of Science, King Saud University, Building 5, Riyadh 11451, Riyadh, Saudi Arabia*
[3]*Chemistry Department, Faculty of Science, Benha University, Fareed Nada St., Benha, Egypt*

Abstract. This study investigates the specific capacitance and electrochemical properties of a charge-transfer (CT) complex formed between 4,4′-bipyridine (BPy) and 2,3-dichloro-5,6-dicyano-1,4-benzoquinone (DDQ), focusing on its potential application as a redox-active component in advanced energy storage systems. A comprehensive series of electrochemical analyses was conducted to elucidate the electronic interactions and capacitive behavior of BPy in the presence of DDQ. Cyclic voltammetry (CV) revealed enhanced pseudocapacitive behavior, attributed to synergistic charge-transfer interactions between the nitrogen centers of BPy and the electron-deficient carbonyl groups of the nonequivalent derivative. The presence of C≡N and Cl substituents on the quinone ring was found to significantly influence the redox potentials and modulate the π–π* and n–π* charge-transfer processes, thereby affecting the electron density distribution within the molecular complex. Notably, the BPy–DDQ complex exhibited a high specific capacitance, reaching up to 114 F/g at a scan rate of 0.4 V/s, which is ascribed to enhanced charge delocalization and improved interfacial conductivity. Morphological analysis using scanning and transmission electron microscopy (SEM and TEM) further revealed the nanostructured features of the CT complex. These findings highlight the potential of BPy–DDQ complex as tunable, redox-active materials for next-generation supercapacitors and other electrochemical energy storage applications.

***Keywords*:** specific capacitance; pseudocapacitive; cyclic voltammetry; DDQ; BPy.

1. Introduction

The growing demand for efficient and sustainable energy storage technologies has spurred intense research into the development of advanced materials capable of delivering high energy and power densities. Organic charge-transfer (CT) complexes, particularly those formed between 4,4′-bipyridine (BPy) and benzoquinone (BQ) derivatives, have emerged as promising candidates due to their intrinsic redox activity, structural tunability, and favorable electrochemical behavior. BPy, a nitrogen-containing heterocyclic compound, functions as a strong electron-donating ligand, while BQ derivatives, characterized by electron-deficient carbonyl groups, act as effective electron acceptors. The interaction between these donor–acceptor pairs results in the formation of CT complexes with reversible redox properties, making them highly attractive for applications in energy storage systems such as supercapacitors and organic rechargeable batteries [1].

Among various energy storage technologies, secondary batteries play a pivotal role in advancing clean and renewable energy strategies [2]. Organic electrode materials have gained attention due to their flexible molecular design, broad availability of raw materials, and compatibility with various ion transport mechanisms, often being amorphous and insensitive to ionic radii [3]. Four major classes of organic redox-active materials have been reported: conducting polymers [4], organic radicals [5], organodisulfides [6], and conjugated carbonyl compounds [7]. Of these, conjugated carbonyl compounds stand out as classic redox-active materials, offering high theoretical capacities, fast kinetics, and multi-electron transfer capabilities. Since their introduction in 1969 as battery electrodes [8–15], quinone-based molecules have been extensively studied for their excellent redox reversibility and structural adaptability. Notably, *p*-benzoquinone, the simplest of this class, provides high energy density and electronic stability [16–19]. However, its practical application has been limited by two major drawbacks: high solubility in electrolytes, which leads to capacity fading, and a relatively low operating voltage (< 2.4 V), which restricts energy density [20-22].

To address these challenges, several strategies have been employed, including structural modifications through the incorporation of various substituents-such as alkyl groups [23], lithium phenolates [24], sulfonates [25], and alkoxy groups-to enhance molecular interactions and reduce solubility [26]. However, these substituents are often electrochemically inactive and may compromise overall performance [27]. Efforts to improve cycling stability through the design of BQ oligomers or the formation of direct C–C linkages between BQ units have also been explored, however,

[*] Corresponding author. *E-mail address:* i.elhallag@yahoo.com (Ibrahim El-Hallag)

these approaches frequently suffer from limited redox site utilization or diminished capacity due to steric hindrance and repulsive interactions [28–30].

An alternative approach involves enhancing π–π interactions within the molecular framework to improve charge delocalization and cycling performance [31]. For example, 1,4-bis(*p*-benzoquinonyl)benzene and 1,3,5-tris(*p*-benzoquinonyl)-benzene have demonstrated promising capacities and structural adaptability, although challenges such as limited voltage windows and poor long-term stability persist. Despite notable progress, further improvements are needed to fully realize the full potential of organic redox-active materials [32]. In this context, specific capacitance emerges as a key metric for evaluating charge storage capabilities in CT-based systems. It quantifies the ability of a material to store electric charge per unit mass, area, or volume and can be assessed via electrochemical techniques such as cyclic voltammetry and galvanostatic charge–discharge (GCD) [33]. In CT complexes, the specific capacitance provides insight into redox reversibility, electron/ion transport dynamics, and interfacial conductivity.

In this study, we investigates the capacitive behavior and electrochemical performance of a CT complex formed between BPy and a substituted benzoquinone derivative, *i.e.*, 2,3-dichloro-5,6-dicyano-1,4-benzoquinone (DDQ). Cyclic voltammetry was employed to evaluate redox characteristics and estimate specific capacitance, while scanning electron microscopy (SEM) and transmission electron microscopy (TEM) were used to assess morphological features. Additionally, the influence of molecular structure on charge transfer behavior was examined to guide the design of redox-active organic materials for energy storage devices.

2. Experimental

2.1. Materials

All chemicals were of analytical reagent grade and used without further purification. Solvents were purified and dried following standard procedures. 2,3-Dichloro-5,6-dicyano-1,4-benzoquinone (DDQ) and 4,4′-bipyridine (BPy) were purchased from Aldrich Chemical Co. and used as received.

2.2. Synthesis of the solid charge transfer complex

A 1:1 molar mixture of 4,4′-bipyridine (3.0 mmol) and DDQ (3.0 mmol) was dissolved in ethanol to form the CT complex. The resulting solution was stirred at room temperature, and the precipitated solid complex was collected by filtration. The solid was then thoroughly washed with small volumes of ethanol and dried under vacuum to yield the BPy–DDQ CT complex (Fig. 1).

2.3. Electrochemical measurements

Electrochemical studies were carried out using a standard three-electrode cell configuration. The working electrode was a gold disc (surface area = 6.75 × 10^{-3} cm^2), the reference electrode was Ag/AgCl (saturated KCl), and a coiled platinum wire served as the counter electrode. CV was performed using the EG&G Potentiostat Model 283. All measurements were conducted at room temperature (23 ± 2 °C) in an anhydrous dichloromethane (CH_2Cl_2) solution containing 0.1 M tetraethylammonium perchlorate (TEAP) as the supporting electrolyte. Scan rates ranged from 0.025 to 1.0 V s^{-1} to study the redox kinetics of the 2 mM CT complex. Prior to each measurement, the solution was thoroughly purged with oxygen-free nitrogen for at least 15 minutes, and a nitrogen blanket was maintained throughout the experiments to prevent oxygen interference.

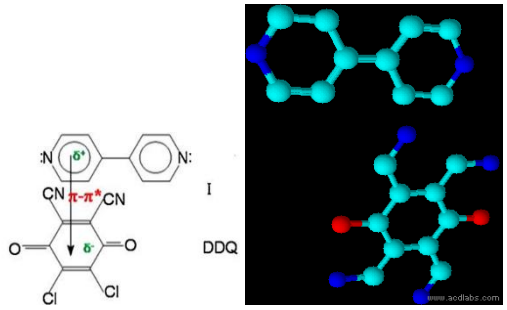

Figure 1. Skeletal structure of the BPy-DDQ CT complex.

3. Results and discussion

3.1. Cyclic voltammetry

The cyclic voltammetry profiles of the 4,4′-bipyridine–benzoquinone (Bpy-BQ) CT complex revealed distinct redox peaks, confirming the formation of stable CT complexes. The peak current and peak-to-peak separation increased with scan rate, indicating quasi-reversible redox behavior. The peak current ratio (i_{pc}/i_{pa}) was analyzed to assess the reversibility and stability of the CT complex.

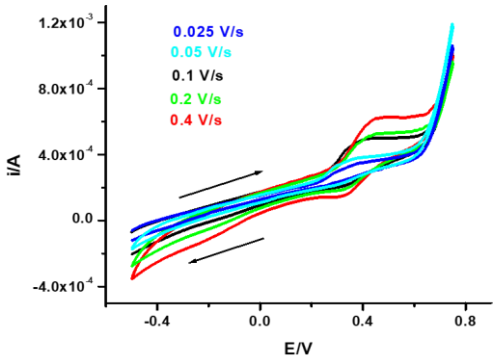

Figure 2. Cyclic voltammograms of the 2 mM BPy–BQ CT complex recorded at a gold electrode in 0.1 M TEAP/CH_2Cl_2 at room temperature, under various scan rates.

The voltammograms shown in Figure 2 exhibited well-defined coupled peaks, which were characterized by an anodic peak in the forward scan and a cathodic peak in the reverse scan. The peak current ratio (i_{pc}/i_{pa}) was found to be less than unity at all scan rates, which, along with persistent peak shapes upon cycling, confirm the electrochemical stability of the *o*-benzoquinone species formed at the electrode surface. This behavior suggests a slow chemical step following the charge transfer within the CV time scale [34]. The shape, position, and peak potential separation ($\Delta E_p = E_{pa} - E_{pc}$) of the voltammograms provide insight into electron transfer kinetics. For a reversible system, ΔE_p

approaches the theoretical value of ~59 mV/n (*n* = number of electrons transferred). In contrast, greater separation and peak asymmetry of the CT-complex are hallmarks of a quasi-reversible system, often scan-rate-dependent due to diffusion limitations. As indicated in Figure 3, the voltammetric current response (i_p) displayed a linear relationship with the square root of the scan rate ($v^{½}$), indicating a diffusion-controlled electron transfer process. A plot of log i_p vs. log ν yielded a slope of ~0.5, further supporting diffusion-controlled behavior. The formal redox potential (E′°), calculated as the average of anodic and cathodic peaks, was found to be 0.393 V. The heterogeneous electron transfer rate constant (k^0) was estimated using literature working curves based on ΔE_p vs. dimensionless parameters and was determined to be $3.9 \pm 0.1 \times 10^{-3}$ cm·s^{-1} [34].

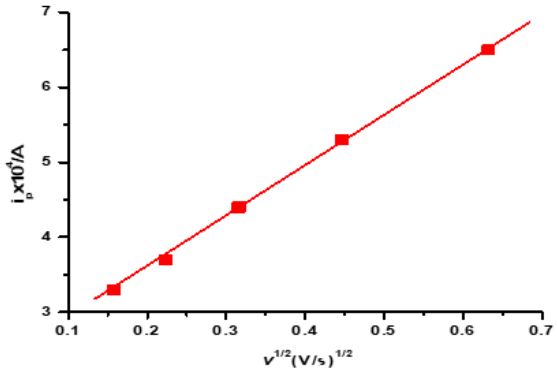

Figure 3. Linear plot of peak current (i_p, µA) versus the square root of scan rate ((ν, V/s)$^{1/2}$); the data follow the regression equation $i_p = 6.81\ v^{1/2} + 2.22$ with a high coefficient of determination ($R^2 = 0.999$).

3.2. Specific capacitance from cyclic voltammetry

Specific capacitance is a critical parameter for evaluating electrochemical performance in redox-active materials, particularly those designed for energy storage applications such as supercapacitors and pseudocapacitors. The CT complex of BPy and benzoquinone derivatives was evaluated using CV, a technique well-suited for probing redox behavior and charge storage characteristics.

The area enclosed by the CV curve is directly proportional to the total charge (Q) involved in the redox processes. This charge can be used to calculate the specific capacitance (C_{sp}) of the active material via the following equation:

$$C_{sp} = \frac{1}{2mv\Delta V}\int_{V1}^{V2} I(V)dV \qquad (1)$$

where *m* is the mass of the active material deposited on the electrode (1.01 µg), *v* is the scan rate (*V*/s,) , Δ*V* is the potential window (*V*), *I* (*V*) is the current as a function of potential (*V*), and the integral represents the area under the CV curve during a complete cycle for both anodic and cathodic sweeps. The factor of 2 accounts for the full cycle (both anodic and cathodic sweeps). CV measurements were conducted over a potential window of 1.2 V at various scan rates ranging from 0.025 to 0.40 V/s. The integrated area under the CV curve was used to calculate the C_{sp}, summarized in Table 1.

Table 1. Specific capacitance values of BPy-BQ complex at various scan rates compared with representative values reported in the literature.

Scan rate (V/s)		Specific capacitance (F/g)		Reference
This work	Reported in literature	This work	Reported in literature	
0.025	0.01-0.1	494	311-702	[35]
0.05	0.01-0.05	360	180-360	[36]
0.1	0.05	303	303.5	[37]
0.2	— *	231	1405	[38]
0.4	— **	114	1087	[39]

* Reference 38 reports the specific capacitance determined using the constant-current charge–discharge (galvanostatic) method (1405 F/g); therefore, no scan rate is applicable.
** Reference 39 reports a specific capacitance of 1087 F/g, also determined using the constant-current charge–discharge (galvanostatic) method; therefore, no scan rate is applicable.

As shown in the above table, the variation of specific capacitance (C_{sp}) with scan rate in this work is consistent with the expected behavior of charge-transfer-based pseudocapacitive systems, where C_{sp} decreases as the scan rate increases due to restricted ion diffusion and limited time for redox interactions. At a scan rate of 0.025 V/s, the C_{sp} value of 494 F/g is well within the reported literature range of 311–702 F/g [35], indicating efficient utilization of electroactive sites at lower scan rates. Similarly, at 0.05 V/s, the C_{sp} reaches 360 F/g, matching the upper limit of the reported range (180–360 F/g) [36], reflecting the favorable electrochemical kinetics of the synthesized material. At 0.1 V/s, the observed C_{sp} (303 F/g) is in excellent agreement with the literature value of 303.5 F/g [37], further validating the consistency and reproducibility of the electrochemical response. At higher scan rates, such as 0.2 V/s and 0.4 V/s, the C_{sp} decreases to 231 F/g and 114 F/g, respectively. While these values are lower than some literature reports (*e.g.*, 1405 F/g [38] and 1087 F/g [39]), it is important to note that those capacitance values were obtained using the constant-current charge–discharge (CCCD) method. CCCD measurements often overestimate capacitance due to longer polarization times, and direct comparisons with CV-derived C_{sp} values must consider differences in methodology and normalization. Overall, the results confirm the high specific capacitance and competitive electrochemical performance of the synthesized charge-transfer complex, especially at low and moderate scan rates.

Further, the decrease in C_{sp} with increasing scan rate suggests a scan rate-dependent charge storage mechanism in the CT complex. At lower scan rates, the slower potential sweep allows sufficient time for diffusion of analyte and complete faradaic reactions at the donor–acceptor interface. This results in enhanced utilization of redox-active sites and higher capacitance. In contrast, at higher scan rates, limited ion diffusion and restricted redox kinetics reduce the active surface accessibility, thereby lowering the observed capacitance. These observations underscore the pseudocapacitive nature of the BPy–BQ complex, driven by quasi-reversible redox transitions between quinone and hydroquinone states. The well-defined redox peaks and their scan-rate dependence support a faradaic charge storage mechanism, distinct from purely double-layer capacitive behavior. Figure 4 displays the plot of specific capacitance versus scan rate, highlighting the dynamic response of the CT complex and illustrating the transition from diffusion-limited faradaic processes at low scan rates to surface-limited capacitive behavior at higher scan rates.

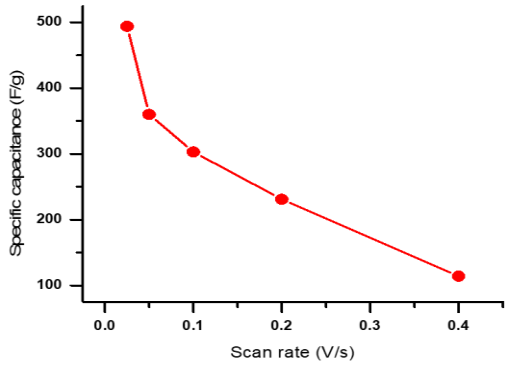

Figure 4. Variation of specific capacitance (C_{sp}) with scan rate for BPy-BQ complex

This mixed behavior—combining faradaic and capacitive contributions—demonstrates the versatility of CT complexes in energy storage applications. Moreover, the high values of specific capacitance at low scan rates emphasize the potential of the BPy–BQ system for applications requiring high energy density and stable cycling performance.

3.3. Double-layer capacitance and electrochemically active surface area

Electrochemical characterization of electrode materials often involves determining interfacial parameters such as double-layer capacitance (C_{dl}) and electrochemically active surface area (ECSA), providing insight into charge accumulation, ion transport, and surface reactivity [40]. Double-layer capacitance originates from the formation of the electrical double layer (EDL) at the electrode–electrolyte interface. This is a non-faradaic process governed by the physical separation of charges at the interface, analogous to a conventional capacitor. C_{dl} can be determined from CV experiments performed in a narrow potential window devoid of faradaic processes, where the current response is predominantly capacitive, using the relationship:

$$i_c = C_{dl} \times \nu \qquad (2)$$

where i_c denotes the capacitive current (A), calculated as the average of anodic and cathodic currents measured at potentials corresponding to non-faradaic processes, and ν represents the scan rate (V/s).

Figure 5 indicates the plotting of i_c versus ν, yielding a straight line with the slope corresponding to C_{dl} *(mF)*. The values of the capacitive current (A), scan rate (V/s) and C_{dl} are summarized in Table 2.

Table 2. Capacitive current and corresponding C_{dl} values for 4,4′-bipyridine–benzoquinone complex

Scan rate (V/s)	Capacitance current (mA)	C_{dl} (mF)
0.025	0.030	1.298
0.05	0.052	
0.10	0.095	
0.20	0.172	
0.40	0.320	

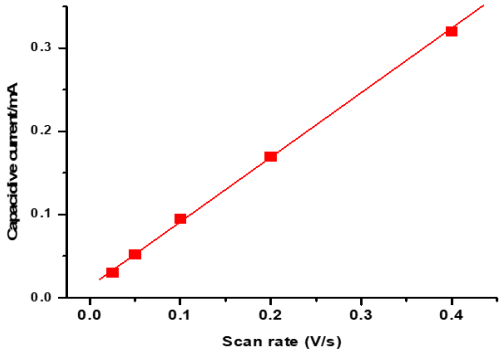

Figure 5. Linear plot of capacitive current (*i*c, mA) versus scan rate (ν, V/s); the regression equation is *i*c = 1.298 ν – 0.019 with R^2 = 0.999.

The obtained C_{dl} value of 1.298 mF reflects a high interfacial charge storage capacity, indicative of a porous, supramolecularly organized electrode surface that facilitates efficient ion access and charge redistribution.

The ECSA can be estimated using the following equation:

$$\text{ECSA} = C_{dl}/C_s \qquad (3)$$

where C_s is the specific capacitance per unit area of a smooth planar electrode (typically 18.359 µF/cm² for non-aqueous systems). Using this approach, the calculated ECSA for the BPy–BQ complex was found to be 70.662 cm², significantly exceeding the geometric surface area. This increase confirms the presence of a highly electrochemically accessible and nanostructured surface, which promotes charge-transfer processes and redox activity. Previous literature reports on CT complexes involving bipyridine and quinone derivatives highlight similar findings, attributing the enhanced electrochemical properties to π–π stacking interactions and hydrogen bonding [41-49]. These molecular interactions contribute to increased surface area and redox reversibility. Thus, C_{dl} and ECSA serve as valuable proxies for assessing the real electroactive interface in CT-based materials. Their determination is especially important in nanoporous electrodes, where geometric surface measurements severely underestimate the true reactive area. In conclusion, the high specific

capacitance, elevated C_{dl}, and large ECSA of the 4,4′-bipyridine–benzoquinone complex confirm its strong pseudocapacitive behavior, efficient ion transport, and electrochemical reversibility. These findings underscore the potential of CT complexes for next-generation energy storage applications, including electrochemical sensors, biointerfaces, and hybrid energy conversion systems. Monitoring specific capacitance as a function of scan rate not only aids in mechanistic understanding but also serves as a critical design criterion for optimizing the performance of advanced redox-active materials.

3.4. Surface morphology analysis

The surface morphology of the synthesized 4,4′-bipyridine–benzoquinone CT complex was examined using scanning electron microscopy (SEM) to elucidate its microstructural organization and topographical characteristics. The CT complex was prepared via slow solvent evaporation from a 1:1 ethanol–water mixture at ambient conditions a strategy conductive to supramolecular self-assembly driven by π–π stacking and charge-transfer interactions between the donor (4,4′-bipyridine) and acceptor (benzoquinone) molecules.

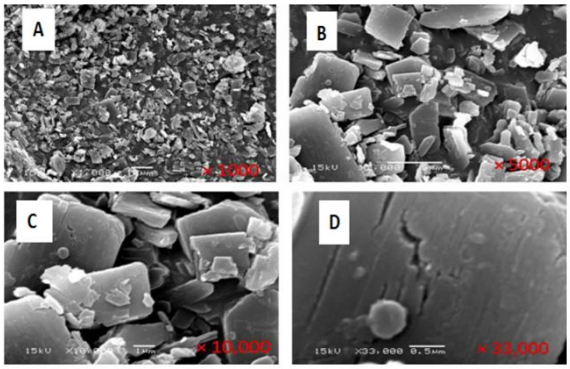

Figure 6. The scanning electron microscope (SEM) for BPy-DDQ at different magnifications.

As shown above, Figure 6 presents SEM micrographs of the BPy–BQ complex at various magnifications. At low magnification (Figure 6A; ×1,000, scale bar = 10 µm), the surface exhibits a heterogeneous distribution of irregular, microcrystalline aggregates dispersed across the substrate, indicating uniform film formation. The overall rough texture and granular morphology suggest an interconnected, porous structure that may facilitate efficient electrolyte penetration and ion diffusion. With increased magnification (Figure 6B; ×5,000, scale bar = 3 µm), well-defined platelet-like crystallites emerge, displaying angular edges and layered stacking—features typically associated with anisotropic crystal growth guided by directional donor–acceptor interactions and intermolecular hydrogen bonding. At ×10,000 magnification (Figure 6C; scale bar = 1 µm), compact prismatic structures become more apparent, with distinguishable facets and overlapping domains. Some crystals exhibit fractured surfaces, possibly arising from stress differentials during solvent evaporation or lattice expansion during growth. Smaller flakes or fragments attached to the surfaces of larger crystals may indicate secondary nucleation or reorganization during drying. At the highest resolution (Figure 6D; ×33,000, scale bar = 0.5 µm), nanoscale surface features such as striations, cracks, and textural heterogeneities are clearly visible. These fine structural irregularities are likely the result of internal lattice strain, solvent-induced stress, or interfacial defects, and they may play a critical role in enhancing electrochemical behavior by increasing the density of active surface sites.

The morphological features revealed by SEM—particularly the platelet-like geometry, hierarchical stacking, and nanoscale cracks—suggest the presence of a high density of electrochemically accessible sites. This structural interpretation is corroborated by electrochemical measurements. CV performed in a non-faradaic potential window was used to extract the double-layer capacitance (C_{dl}) through linear fitting of capacitive current versus scan rate. A C_{dl} value of 1.298 mF was obtained, which corresponds to an electrochemically active surface area (ECSA) of 70.662 cm², assuming a specific capacitance (C_s) of 18.359 µF/cm² for a smooth electrode in non-aqueous media. These quantitative values reinforce the morphological findings, confirming that the CT complex film exhibits a significantly enhanced electroactive surface area relative to its geometric footprint [49]. The hierarchical roughness, combined with interfacial defects and crystal anisotropy, likely contributes to the observed pseudocapacitive behavior. Such features enable efficient ion transport and rapid redox transitions, thereby supporting the material's high electrochemical performance.

3.5. Microstructural analysis

To complement the SEM findings and gain deeper insight into the internal nanostructure of the CT complex, transmission electron microscopy (TEM) analysis was conducted. The representative TEM image is shown in Figure 7.

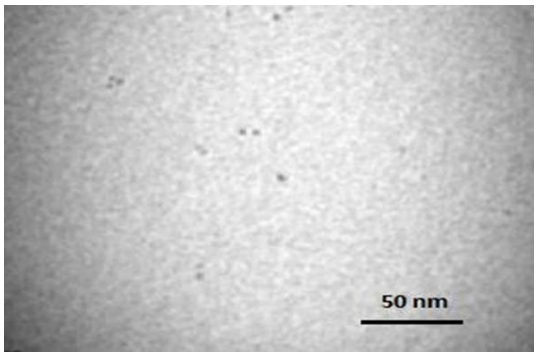

Figure 7. Transmission electron microscopy (TEM) image of the 4,4′-bipyridine–benzoquinone charge-transfer complex.

The micrograph reveals a relatively homogeneous matrix with subtle variations in contrast, suggesting a largely amorphous or finely dispersed nanostructure. The absence of discernible lattice fringes or well-defined crystalline domains indicates that the CT complex predominantly adopts a non-crystalline or poorly ordered configuration under the imaging conditions employed. This is consistent with the hypothesis that molecular-level interactions rather than long-range crystallinity dominate the structural

organization of the BPy–BQ system. The micrograph indicates a predominantly amorphous or molecularly dispersed morphology, with no discernible lattice fringes. The presence of sporadic dark contrast regions suggests localized variations in electron density, which may be attributed to π–π stacking interactions or the formation of small donor–acceptor aggregates.

Scattered darker regions or spots are observed across the field of view, which may correspond to localized domains of increased electron density, such as small aggregates or clusters arising from π–π stacking between bipyridine and benzoquinone units. These regions likely represent nanoscale ordering driven by donor–acceptor interactions, although they are not extensive enough to produce sharp crystalline features.

The observed amorphous or semi-ordered morphology supports the interpretation that the CT complex forms a continuous, molecularly interpenetrated film rather than discrete crystalline phases [50]. This kind of microstructure may be advantageous for electrochemical applications, as it facilitates uniform ion accessibility, promotes consistent redox activity across the film, and enhances interfacial contact with the electrolyte. Such characteristics contribute to the stable and efficient charge storage behavior observed in the cyclic voltammetry results. The lack of crystallinity implies a homogeneous internal morphology that favors uniform electrochemical performance.

4. Conclusions

The electrochemical characterization of the 4,4′-bipyridine–benzoquinone (BPy–BQ) charge transfer complex revealed favorable features for pseudocapacitive energy storage applications. Cyclic voltammetry exhibited quasi-rectangular profiles superimposed with well-defined, reversible redox peaks—indicative of a hybrid charge storage mechanism combining electric double-layer capacitance and fast faradaic reactions. From the slope of capacitive current versus scan rate in the non-faradaic region, a double-layer capacitance (C_{dl}) of 1.298 mF was determined. This corresponds to an electrochemically active surface area of 70.662 cm², based on an assumed specific capacitance of 18.359 μF/cm² for a planar electrode in aqueous media. These values highlight the substantial surface accessibility and efficient charge transport facilitated by the donor–acceptor architecture and supramolecular assembly of the CT complex. The observed pseudocapacitive behavior, governed by rapid interfacial redox kinetics and enhanced π–π stacking interactions, underscores the promise of such molecular CT systems as solution-processable electrode materials for high-performance supercapacitors and hybrid energy storage technologies. The SEM images of the CT complex displayed a homogeneous, rough surface with micro aggregated domains, indicating effective complexation. TEM analysis revealed nanoscale features and amorphous zones, supporting the formation of disordered yet conductive CT networks. Lattice contrast variations suggested partial crystallinity, which may enhance electron delocalization across donor–acceptor interfaces. Overall, the morphology observed via SEM and TEM confirms the structural foundation for efficient charge transport in the CT complex. Although the BPy–DDQ complex exhibited promising pseudocapacitive behavior, the present investigation was conducted using a single-electrode configuration in a non-aqueous electrolyte system. Such a configuration is useful for fundamental studies but does not reflect practical device conditions. To evaluate the real-world applicability of this material, further testing is required under full-cell configurations using symmetric or asymmetric two-electrode systems. In addition, assessing performance in aqueous or solid-state electrolytes and conducting long-term cycling stability tests are necessary to confirm its potential for practical electrochemical energy storage applications.

Conflict of interest

The authors declare that they have no conflict of interest.

References

[1]. S. Cao, H. Zhang, Y. Zhao, Y. Zhao, Pillararene/ Calixarene-based systems for battery and supercapacitor applications, Science 1 (2021) 28–43. DOI: 10.1016/j.esci.2021.10.001

[2]. X. Yin, S. Sarkar, S. Shi, Q.A. Huang, H. Zhao, L. Yan, Y. Zhao, J. Zhang, Recent progress in advanced organic electrode materials for sodium-ion batteries: synthesis, mechanisms, challenges and perspectives, Advanced Functional Materials 30 (2020) 1908445. DOI: 10.1002/ adfm. 201908445

[3]. Y. Liang, Z. Tao, J. Chen, Organic electrode materials for rechargeable lithium batteries, Advanced Energy Materials 2 (2012) 702–702. DOI: 10.1002/aenm.201100795

[4]. J. Yang, Y. Shi, P. Sun, P. Xiong, Y. Xu, Optimization of molecular structure and electrode architecture of anthraquinone-containing polymer cathode for high-performance lithium-ion batteries, ACS Applied Materials &. Interfaces 11 (2019) 42305–42312. DOI: 10.1021/acsami. 9b16678

[5]. K. Oyaizu, T. Sukegawa, H. Nishide, Dual dopable poly(phenylacetylene) with nitronyl nitroxide pendants for reversible ambipolar charging and discharging, Chemical Letters 40 (2011) 184–185. DOI: 10.1246/cl.2011.184

[6]. S. Akay, B. Esat, I. Fidan, C. Hirel, N. Frank, New benzimidazole nitronyl nitroxides as electro-active compounds for battery electrodes, ECS Meeting Abstracts, MA. 2014-04 (2014) 391–391.

[7]. T. Nokami, T. Matsuo, Y. Inatomi, N. Hojo, T. Tsukagoshi, H. Yoshizawa, A. Shimizu, H. Kuramoto, K. Komae, H. Tsuyama, J. Yoshida, Polymer-bound pyrene-4,5,9,10-tetraone for fast-charge and -discharge lithium-ion batteries with high capacity, Journal of the American Chemical Society 134 (2012) 19694–19700. DOI: 10.1021/ja306663g

[8]. W. Huang, S. Zheng, X. Zhang, W. Zhou, W. Xiong, J. Chen, Synthesis and application of calix[6]quinone as a high-capacity organic cathode for plastic crystal electrolyte-based lithium-ion batteries, Energy Storage Materials 26 (2020) 465–471. DOI: 10.1016/j.ensm.2019.1

[9]. M. Lee, J. Hong, B. Lee, K. Ku, S. Lee, C.B. Park, K. Kang, Multi-electron redox phenazine for ready-to-charge organic batteries, Green Chemistry 19 (2017) 2980–2985. DOI: 10.1039/ C7GC01378E

[10]. F. Strauss, D. Kitsche, Y. Ma, J.H. Teo, D. Goonetilleke, J. Janek, M. Bianchini, T. Brezesinski, Operando characterization techniques for all-solid-state lithium-ion batteries, Advanced Energy and Sustainability Research 2 (2021) 2100004. DOI: 10.1002/aesr.202100004

[11]. Y. Tong, X. Wang, Y. Zhang, W. Huang, Recent advances of covalent organic frameworks in lithium-ion batteries, Inorganic Chemistry Frontiers 8 (2021) 558–571. DOI: 10.1039/D0QI01104E

[12]. H. Wang, C.J. Yao, H.J. Nie, K.Z. Wang, Y.W. Zhong, P. Chen, S. Mei, Q. Zhang, Recent progress in carbonyl-based organic polymers as promising electrode materials for lithium-ion batteries (LIBs), Journal of Materials Chemistry A 8 (2020) 11906–11922. DOI: 10.1039/D0TA03321A

[13]. J. Xie, Q. Zhang, Recent progress in multivalent metal (Mg, Zn, Ca, and Al) and metal-ion rechargeable batteries with organic materials as promising electrodes, Small 15 (2019) e1805061. DOI: 10.1002/smll.201805061

[14]. W. Xiong, W. Huang, M. Zhang, P. Hu, H. Cui, Q. Zhang, Pillar[5]quinone–carbon nanocomposites as high-capacity cathodes for sodium-ion batteries, Chemistry of Materials 31 (2019) 8069–8075. DOI: 10.1021/acs.chemmater.9b02601

[15]. Y. Zhang, Z. Sun, X. Kong, Y. Lin, W. Huang, An all-organic symmetric battery based on a triquinoxalinylene derivative with different redox-voltage active sites and a large conjugation system, Journal of Materials Chemistry A 9 (2021) 26208–26215. DOI: 10.1039/D1TA08637K

[16]. Z. Luo, L. Liu, Q. Zhao, F. Li, J. Chen, An insoluble benzoquinone-based organic cathode for use in rechargeable lithium-ion batteries, Angewandte Chemie International Edition 56 (2017) 12561–12565. DOI: 10.1002/anie. 201706604

[17]. X. Cao, J. Liu, L. Zhu, L. Xie, Polymer electrode materials for high-performance lithi-um/sodium-ion batteries: a review, Energy Technology 7 (2019) 1800759. DOI: 10.1002/ente.201800759

[18]. L. Zhu, G. Ding, L. Xie, X. Cao, J. Liu, X. Lei, J. Ma, Conjugated carbonyl compounds as high-performance cathode materials for rechargeable batteries, Chemistry of Materials 31 (2019) 8582–8612. DOI: 10.1021/acs.chemmater.9b03109

[19]. L.M. Zhu, G.C. Ding, Q. Han, Y.X. Miao, X. Li, X.L. Yang, L. Chen, G.K. Wang, L.L. Xie, X.Y. Cao, Enhancing electrochemical performances of small quinones toward lithium and sodium energy storage, Rare Metals 41 (2022) 425–437. DOI**:** 10.1007/s12598-021-01890-5

[20]. X. Wang, Z. Shang, A. Yang, Q. Zhang, F. Cheng, D. Jia, J. Chen, Combining quinone cathode and ionic liquid electrolyte for organic sodium-ion batteries, Chem 5 (2019) 364–375. DOI: 10.1016/j.chempr.2018.10.018

[21]. Y. Lu, Q. Zhang, L. Li, Z. Niu, J. Chen, Design strategies toward enhancing the performance of organic electrode materials in metal-ion batteries, Chem 4 (2018) 2786–2813 DOI: 10.1016/j.chempr.2018.09.005

[22]. T. Yokoji, Y. Kameyama, S. Sakaida, N. Maruyama, M. Satoh, H. Matsubara, Steric effects on the cyclability of benzoquinone-type organic cathode active materials for rechargeable batteries, Chemistry Letters 44 (2015) 1726–1728. DOI: 10.1246/cl.150836

[23]. J. Liu, H. Xia, D. Xue, L. Lu, Double-shelled nanocapsules of V_2O_5-based composites as high-performance anode and cathode materials for Li-ion batteries, Journal of the American. Chemical Society 131 (2009) 12086–12087. DOI: 10.1021/ja9053256

[24]. A.E. Lakraychi, E. Deunf, K. Fahsi, P. Jimenez, J.P. Bonnet, F. Djedaini-Pilard, M. Bécuwe, P. Poizot, F. Dolhem, An air-stable lithiated cathode material based on a 1,4-benzenedisulfonate backbone for organic Li-ion batteries, Journal of Materials Chemistry A 6 (2018)19182–19189. DOI: 10.1039/C8TA06 678F

[25]. M. Yao, H. Senoh, S.I. Yamazaki, Z. Siroma, T. Sakai, K. Yasuda, High-capacity organic positive-electrode material based on a benzoquinone derivative for use in rechargeable lithium batteries, Journal of Power Sources 195 (2010) 8336–8340. DOI: 10.1016/j.jpowsour.2010.06.069

[26]. W. Guo, Y.X. Yin, S. Xin, Y.G. Guo, L.J. Wan, Superior radical polymer cathode material with a two-electron-process redox reaction promoted by graphene, Energy & Environmental Science Energy 5 (2012) 5221–5225. DOI: 10.1039/C1EE02148F

[27]. Y. Wang, Y. Zhang, H. Li, Y. Peng, J. Li, J. Wang, B.-J. Hwang, J. Zhao, Realizing high reversible capacity: 3D intertwined CNTs inherently conductive network for CuS as an anode for lithium-ion batteries, Chemical Engineering Journal 332 (2018) 49–56. DOI: 10.1016/j.cej.2017.09.070

[28]. J.E. Kwon, C.S. Hyun, Y.J. Ryu, J. Lee, D.J. Min, M.J. Park, B.K. An, S.Y. Park, Triptycene-based quinone molecules showing multi-electron redox reactions for large capacity and high-energy organic cathode materials in Li-ion batteries, Journal of Materials Chemistry A. 6 (2018) 3134–3140. DOI: 10.1039/C7TA09968A

[29]. Z. Zhu, M. Hong, D. Guo, J. Shi, Z. Tao, J. Chen, All-solid-state lithium organic battery with composite polymer electrolyte and pillar[5]quinone cathode, Journal of the American

Chemical Society 136 (2014) 16461–16464. DOI: 10.1021/ja507852t
[30]. M. Tang, S. Zhu, Z. Liu, C. Jiang, Y. Wu, H. Li, B. Wang, E. Wang, J. Ma, C. Wang, Tailoring π-conjugated systems: from π–π stacking to high-rate-performance organic cathodes, Chem 4 (2018) 2600–2614. DOI: 10.1016/j.chempr.2018.08.014
[31]. J. Yang, P. Xiong, Y. Shi, P. Sun, Z. Wang, Z. Chen, Y. Xu, Rational molecular design of benzoquinone-derived cathode materials for high-performance lithium-ion batteries, Advanced Functional Materials 30 (2020) 1909597. DOI: 10.1002/adfm.201909597
[32]. P. Poizot, Y. Yao, J. Chen, U.S. Schubert, Preface to the special issue of ChemSusChem on organic batteries, ChemSusChem 13 (2020) 2107–2109. DOI: 10.1002/cssc.202001022
[33]. N. Kumar, S.B. Kim, S.Y. Lee, S.J. Park, Recent advanced supercapacitors: a review of storage mechanisms, electrode materials, modification, and perspectives, Nanomaterials 12 (2022) 3708. DOI: 10.3390/nano12203708
[34]. A.A. Al-Owais, I.S. El-Hallag, E.H. El-Mossalamy, Convolutive–deconvolutive voltammetry of charge-transfer complex of 4,4′-bipyridine with benzoquinone derivatives, Journal. of New Materials for Electrochemical Systems 24 (2021) 195–200. DOI: 10.14447/jnmes.v24i3.a07
[35]. A.A. Al-Owais, I.S. El-Hallag, M.A. Ghanem, E.H. El-Mossalamy, Capacitance properties of electrodeposited polyaniline films on stainless steel substrate, Journal of New Materials for Electrochemical Systems 18 (2015) 017–020. DOI: 383 10.14447/ jnmes.v18i1
[36]. J.K. Jadoon, P.V. Pham, Hybrid TiO_2–RGO nanocomposite as high specific capacitance electrode for supercapacitors, Nanotechnology 35 (2024) 435706. DOI: 10.1088/1361-6528/ad6a6a
[37]. D. Liu, L. Zhou, Y. Liu, C. Xia, J. Ouyang, A.A. Adesina, Electrodeposition fabrication of graphene oxide/α-MnO_2/polyaniline hierarchical porous electrodes with large hybrid specific capacitance for efficient U(VI) electrosorption, Journal of Environmental Chemical Engineering 12 (2024) 113450. DOI: 10.1016/j.jece.2024.113450
[38]. Z. Hu, L. Zu, Y. Jiang, H. Lian, Y. Liu, Z. Li, F. Chen, X. Wang, X. Cui, High specific capacitance of polyaniline/mesoporous manganese dioxide composite using KI–H_2SO_4 electrolyte, Polymers 7 (2015) 1939–1953. DOI: 10.3390/polym7101491
[39]. K.D. Kumar, T. Ramachandran, Y.A. Kumar, A.A.A. Mohammed, M.C. Kang, Hierarchically fabricated nanoflake–rod-like CoMoO–S supported on Ni foam for high-performance supercapacitor electrode material, Journal of Physics and Chemistry of Solids, 185 (2024) 111735. DOI: 10.1016/j.jpcs.2023.111735
[40]. S. Trasatti, O.A. Petrii, Real surface area measurements in electrochemistry, Pure and Applied Chemistry 63 (1992) 711–734.
[41]. D.H. Evans, One-electron and two-electron transfers in electrochemistry and homogeneous solution reactions, Chemical Reviews 108 (2008) 2113–2144. DOI: 10.1021/cr068066l
[42]. K. Amin, L. Mao, Z. Wei, Recent progress in polymeric carbonyl-based electrode materials for lithium- and sodium-ion batteries, Macromolecular Rapid Communications 40 (2019) e1800565. DOI: 10.1002/marc.201800565
[43]. H. Oubaha, J.F. Gohy, S. Melinte, Carbonyl-based π-conjugated materials: from synthesis to applications in lithium-ion batteries, ChemPlusChem 84 (2019) 1179–1214. DOI: 10.1002/cplu.201800652
[44]. A.J. Cohen, P. Mori-Sánchez, W. Yang, Challenges for density functional theory, Chem. Rev. 112 (2012) 289–320. DOI: 10.1021/cr200107z
[45]. J. Ho, A. Klamt, M.L. Coote, Comment on the correct use of continuum solvent models, The Journal of Physical Chemistry A 114 (2010) 13442–13444. DOI: 10.1021/jp107136j
[46]. Y. Zhang, Y. Li, C. Chen, L. Wang, J. Zhang, Design of new hole-transport materials for efficient perovskite solar cells by suitable combination of donor and core groups, Organic Electronics 49 (2017) 255–261. DOI: 10.1016/j.orgel.2017.06.064
[47]. T. Sun, L. Shen, Y. Jiang, J. Ma, F. Lv, H. Ma, D. Chen, N. Zhu, Wearable textile super-capacitors for self-powered enzyme-free smartsensors, ACS Applied Materials & Interfaces 12 (2020) 21779–21787. DOI: 10.1021/acsami.0c05465
[48]. T. Lu, X. Yu, X. Li, J. Qi, S. Huang, Z. Man, H. Zhuo, Zwitterionic polymer-derived nitrogen- and sulfur-co-doped carbon-coated $Na_3V_2(PO_4)_2F_3$ as a cathode material for sodium-ion battery energy storage, New Journal of Chemistry 45 (2021)19391–19401.DOI: 10.1039/D1NJ03779J
[49]. X. Wu, C. Wu, C. Wei, L. Hu, J. Qian, Y. Cao, X. Ai, J. Wang, H. Yang, Highly crystallized $Na_2CoFe(CN)_6$ with suppressed lattice defects as a superior cathode material for sodium-ion batteries, ACS Applied Materials & Interfaces 8 (2016) 5393–5399. DOI: 10.1021/acsami.5b12620
[50]. V. Nampally, M.K. Palnati, N. Baindla, M. Varukolu, S. Gangadhari, P. Tigulla, Charge-transfer complex between o-phenylenediamine and 2,3-dichloro-5,6-dicyano-1,4-benzoquinone: synthesis, spectrophotometric characterization, computational analysis, and biological applications, ACS Omega 7 (2022) 16689–16704. DOI: 10.1021/acsomega.2c01177

Received: 30.10.2025
Received in revised form: 24.12.2025
Accepted: 29.12.2025